IEEE Access
Multidisciplinary | Rapid Review | Open Access Journal

Received 23 July 2025, accepted 7 August 2025, date of publication 18 August 2025, date of current version 22 August 2025.

*Digital Object Identifier 10.1109/ACCESS.2025.3599679*

RESEARCH ARTICLE

# Osteoarthritis Classification Using Hybrid Quantum Convolutional Neural Network

**DEVANSH TIKARIHA, ABDUL MOOMIN, D. JEYAMANI, AND P. RUKMANI**
School of Computer Science and Engineering, Vellore Institute of Technology, Chennai Campus, Chennai 600127, India
Corresponding author: P. Rukmani (rukmani.p@vit.ac.in)

**ABSTRACT** This work explores the integration of quantum computing within a classical Convolutional Neural Network (CNN) framework, leveraging a VGG16 model enhanced with a quantum Convolutional Neural Network (QCNN) for the classification of knee osteoarthritis (OA) severity. A custom quantum layer was incorporated to boost the model's feature extraction capabilities, enabling effective differentiation between healthy and OA-affected knees in medical imaging data. The model utilises the Swish activation function, which combines smoothness and nonlinearity to enhance learning efficiency and gradient flow, which are critical in complex diagnostic tasks. Using a QCNN, this model harnesses the ability of quantum computing to represent high-dimensional data transformations, a novel approach that complements classical CNN layers by exploring patterns that are not captured in traditional networks. The initial results showed a high classification accuracy of 97.26%, suggesting that quantum-enhanced layers can significantly bolster feature extraction and classification in medical diagnostics. Furthermore, multiple variations of pre-trained models with Quantum Convolutional Layers, such as XceptionNet, ResNet, and InceptionNet, were developed and compared in terms of the evaluation metrics that achieved 87.84,89.70, and 86.64, respectively. This hybrid VGG16-QCNN model showed the highest accuracy, demonstrating the potential of QCNNs in advancing the precision and scalability of AI-driven healthcare solutions.

**INDEX TERMS** Quantum convolutional neural network, VGG16, swish activation function, knee osteoarthritis classification, medical imaging, feature extraction, quantum layer, image preprocessing, convolutional neural networks, medical diagnostics, quantum computing, hyperparameter tuning.

## I. INTRODUCTION

Osteoarthritis (OA) is a degenerative disease of the joints. It affects millions of people worldwide, significantly affecting India, where it affects nearly 22% to 39% of the population above 50 years of age, according to the WHO [1]. This disease causes chronic pain, loss of mobility, and considerable disability, resulting in a heavy socioeconomic burden. Early diagnosis is crucial for improving the treatment results. Traditional approaches, although relying on the analysis of X-rays or MRI images, remain subjective and imprecise. Deep learning technologies, specifically Convolutional Neural Networks (CNNs), have revolutionised medical imaging analysis by automatically classifying images into their corresponding feature categories, and, hence, can be more consistent and effective.

Deep learning has been useful for medical imaging, particularly for classification. CNNs, such as VGG16, excel in feature extraction, enabling the robust analysis of medical images. For OA classification, CNNs can be trained on labelled imaging datasets to recognize the severity patterns. However, medical imaging often involves subtle and complex patterns that traditional CNNs cannot capture. By incorporating quantum circuits that allow for complex state transformations, QCNNs can potentially enhance the feature extraction and improve the classification of OA severity.

Recent developments in quantum machine learning have proven that quantum circuits can represent complex data structures via high-dimensional Hilbert space transformations with increased expressivity and fewer parameters [2].

The associate editor coordinating the review of this manuscript and approving it for publication was Asadullah Shaikh.

For medical imaging applications, where the features in radiographs are subtle and nonlinear, such as knee OA, this becomes particularly useful. Through the incorporation of a quantum convolutional layer within a VGG16 architecture, which seeks to learn more informative correlations in features through entanglement and quantum rotations. Earlier work on brain tumour [3] and heart disease classification [4] confirmed the efficiency of such cross-disciplinary quantum-classical models in enhancing diagnostic accuracy over classical CNNs alone. Our combined strategy is used to improve diagnostic precision through the combined effect of quantum computing and deep learning, leading to a stronger and more scalable system for clinical decision-making.

*Objectives:*

A) To develop a VGG16-QCNN hybrid model for the classification of knee osteoarthritis based on medical imaging data.

B) To assess the accuracy and effectiveness of this model in differentiating between ''Healthy'' and ''Affected'' knee images.

C) To evaluate the potential of quantum-enhanced layers in improving feature extraction and classification within a CNN framework.

D) To investigate the impact of the Swish activation function, which enhances model learning efficiency and gradient flow, in the context of knee osteoarthritis classification.

E) To conduct comparative analyses with other Quantum CNN variations using different pre-trained models and activation function combinations, assessing their relative performance in OA diagnostics.

The key contributions of this work are summarized below:

A novel hybrid quantum-classical model (VGG16-QCNN) is proposed that integrates quantum layers using angle encoding and cyclic entanglement to enhance feature learning. A detailed comparative analysis between various pretrained networks was conducted, and an ablation study compares the impact of activation functions across classical and hybrid architectures. The proposed hybrid model demonstrates improved classification performance with 97.26% accuracy and reduced memory usage. A reproducible evaluation framework is provided for benchmarking hybrid quantum-classical networks in medical image analysis.

The remainder of this paper is organized as follows. Section II provides an overview of existing osteoarthritis classification methods. Section III outlines the system model used in this study. The proposed hybrid experimental setup is described in Section IV. Finally, Section V concludes the study with key observations and future directions.

## II. LITERATURE REVIEW

### A. CNN AND HYBRID DIAGNOSTIC SYSTEMS APPROACHES FOR KNEE OA DETECTION

Recent works have demonstrated the adaptability of neural networks across diverse fields such as control systems, industrial vision and aviation. They have been successfully utilized in the robust control of electromechanical systems [5], [6] high-precision industrial defect detection using Convolutional Neural Networks (CNN) [7]; and gain scheduling for flight control in nonlinear, safety-critical environments [8].

CNNs have proven to be an extremely effective method for OA classification based on X-ray images. In one study, it was possible to achieve a remarkable 98% accuracy with an expertly designed CNN, bettering state-of-the-art models such as Xception and InceptionResNetV2 on all evaluation metrics, that is, precision, recall, F1-score, and accuracy. This proves the ability of CNNs to learn features from X-ray images of knees and confirms the use of traditional backbones, such as VGG16, in our model [9].

Other works utilized YOLOv2 for knee joint detection and a VGG-19 Kellgren-Lawrence grading fine-tuned model and reported a best-case accuracy of 69.7% and a mean absolute error of 0.344 on the OAI dataset. Similarly, transfer learning using VGG-19, ResNet-34, and DenseNet resulted in an accuracy of 98% and a quadratic weighted kappa of 0.99 [10]. These results collectively validate the use of VGG-based models, for example, VGG16, as suitable initial points for OA image classification.

Other studies have examined machine-learning models for OA diagnosis. One used X-ray images with preprocessing and feature extraction, followed by Naive Bayes and Random Forest classifiers to obtain 82.98% accuracy using the OAI dataset [11].

Another study used a multilayer perceptron on sEMG signals with 99.5% accuracy [12]. Extending the application of OA diagnosis using imaging, a recent study used deep models on radiographic data such as computed tomography and X-ray imaging for radiographic hip osteoarthritis (rHOA) diagnosis [13]. The authors suggested a summation CT-AP strategy using pre-trained ResNet18 models and demonstrated that the combination of computed tomography and X-ray images significantly enhanced the detection quality. Model-3, in particular, had a balanced accuracy of 82.2% and an ROC AUC of 0.93, demonstrating its ability to differentiate between rHOA and non-rHOA cases, particularly in sparse training samples.

In another attempt, the utility of magnetic resonance imaging (MRI) for the prediction of knee OA progression was evaluated using deep learning models trained on a large image database of 9,280 images in the OAI database [14]. The ROC AUC accuracy of the classification model was 65%, which was superior to that of 58.7% trained radiologists. The addition of clinical measures, such as the WOMAC pain index, enabled the model to predict pain levels at a 72% ROC AUC. These findings demonstrate the ability of AI to augment clinical decision-making by classifying patients at risk of OA progression. On the other hand, gait-based OA diagnosis has also emerged in the latest research.

A recent study proposed a strong deep learning model for human gait analysis to track OA behavior. The approach used pretrained convolutional neural networks with transfer learning to acquire discriminative features, which were further

augmented with a new probabilistic aggregation method. The extracted features were classified using a kernel extreme learning Machine with more than 96% accuracy on the CASIA B gait database [15]. The results demonstrate the ability of deep feature aggregation to outperform conventional approaches in gait-based OA monitoring. Even with such high performance for each modality, conventional models do not possess the feature extraction capability of deep models, further encouraging the combination of CNNs with more capable building blocks, such as quantum circuits.

Recent advances in deep learning have explored hybrid architectures to enhance the performance of CNNs. Li et al. [16] combined graph structures with LSTMs for improved emotion recognition, while Chebyshev pooling was introduced to retain richer contextual features [17]. A recurrent CNN for sentence classification, capturing long-range dependencies with reduced complexity [18]. These innovations demonstrate how integrating specialized layers, such as graph-based, probabilistic, or sequential, can improve feature extraction, supporting our approach to incorporating quantum convolutional layers for complex medical imaging tasks.

### B. QUANTUM MACHINE LEARNING IN HEALTHCARE IMAGING

Quantum computing is being increasingly applied to medical image analysis. A study with Quantum Convolutional Neural Networks (QCNNs) on the HAM10000 skin lesion dataset, using MobileNet features and quantum encoding, reported an accuracy of 82.86%, which is better than classical models such as ResNet50 and DenseNet121 [19].

Another study applied Fully Convolutional Quantum Neural Networks (FCQ-CNN) for the detection of ischemic heart disease with 84.6% accuracy and better feature mapping [4]. These examples point out the potential of quantum-augmented models for processing high-dimensional and complex medical imaging tasks. Other research has shown hybrid quantum-classical CNNs to outperform a single CNN for brain tumor classification with 89.56% accuracy, high precision, and recall [3].

Quantum models have also been employed to predict heart disease, ovarian tumor classification, and rheumatoid arthritis diagnosis, with improved diagnostic performance through quantum circuit integration [20], [21], [22], [23], [24],confirming the applicability of quantum machine learning to diagnosis in medicine and confirming our justification for using VGG16 with quantum convolutional layers for stable knee OA classification. Earlier research has confirmed the performance and limitations of CNNs, conventional ML models, and new quantum approaches to OA detection and other clinical imaging applications.

The novelty of this work lies in the integration of a proven CNN backbone (VGG16) with quantum convolution to improve feature extraction and classification performance. Our VGG16-QCNN model is one of the first to integrate quantum circuits in a hybrid framework for knee OA diagnosis on real-world data, such as OAI, in a quest for both performance and clinical applicability. The major advantage of Quantum Convolution is its advanced feature detection using Q-bits, gates, and circuits. This advanced feature extraction and recognition method can significantly improve our accuracy over conventional deep learning methods.

## III. PROPOSED METHOD

The proposed hybrid VGG16-QCNN is formed primarily by combining the two conventions of VGG16 and QCNN to obtain optimal results. The Swish activation function [25] is proposed to maximize the model's accuracy for the final classification. The classification algorithm is discussed in Table 3. The architecture diagram of the proposed Hybrid model is depicted below in Figure 1.

### A. PREPROCESSING MEDICAL IMAGES

The process begins with the acquisition and preprocessing of knee joint medical images. Images were normalized and resized to a consistent resolution to ensure compatibility with the VGG16-based Quantum CNN (QCNN) model. Conventional image-processing techniques, such as rotation and scaling, can be applied to prevent overfitting. The proposed hybrid model works with binary classification. Kellgren-Lawrence (KL) Grades 1 and 2 are the early and mild phases of osteoarthritis (OA), and while clinically relevant, they present intrinsic difficulties in automated classification tasks due to their blurry visual features and minimal inter-reader agreement by radiologists. Grades 1 and 2 tended not to have clear-cut radiographic features, resulting in subjective annotations, which may introduce noise into the learning process.

Our main aim was to evaluate the discriminative ability of the hybrid VGG16-QCNN model in separating normal and severely affected knees, which concentrated on grades 0, 3, and 4, where radiographic signs were more distinguishable and annotations tended to be more dependable. Additionally, to obtain a strong binary classification model and prevent class imbalance, we chose more distinct class boundaries, where Grade 0 was mapped to class 0 (non-OA), and grades 3 and 4 were mapped to class 1 (OA). Future studies will focus on multiclass generalizations and methods for a better description of subtle features in early-stage OA with enhanced quantum feature extraction.

Therefore, the OA grade classes were reduced from 5 to 2, as healthy and affected, respectively, as shown in Tables 1 and 2. The input image was a pre-processed X-ray image of the knee joint.

It was resized and normalized for the model, and a false-color color map was applied to improve the contrast. Figure 2 shows an image of the Grade 0 class (healthy). The characteristics observed here included a well-defined joint space with no narrowing. Smooth bone surfaces without visible bone spurs (osteophytes).

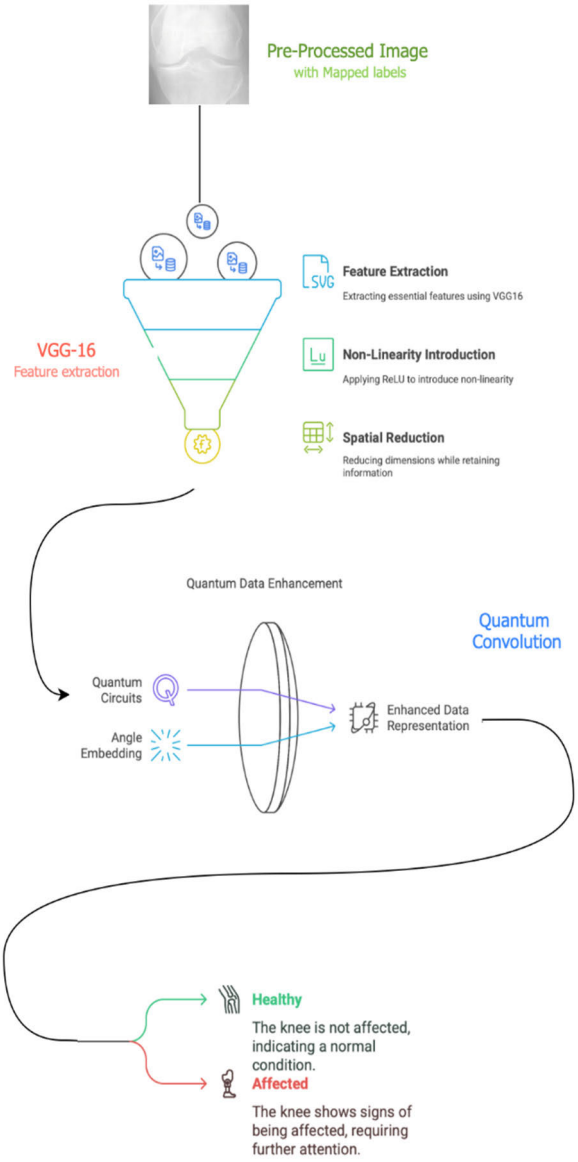


**FIGURE 1.** The Architecture diagram of the proposed model.

**TABLE 1.** Mapping of kellgren-lawrence (KL) grades to binary class labels.

| Grade | Description | Class Label |
|---|---|---|
| Grade 0 | Healthy (no signs of OA) | 0 |
| Grade 1 | Doubtful OA (mild joint space narrowing) | 1 |
| Grade 2 | Minimal OA (moderate joint space narrowing) | 2 |
| Grade 3 | Moderate OA (significant joint space narrowing) | 3 |
| Grade 4 | Severe OA (complete joint space obliteration) | 4 |

### B. FEATURE EXTRACTION WITH VGG16 LAYERS

The preprocessed images were then passed through the initial layers of the pretrained VGG16 model. These layers

**TABLE 2.** Modified binary labelling for the classification task.

| Class | Mapped Label | Preprocessing Step |
|---|---|---|
| Healthy (Grade 0) | 0 | Retained as Grade 0 |
| Affected (Grade 3) | 1 | Mapped to Affected (1) |
| Affected (Grade 4) | 1 | Mapped to Affected (1) |

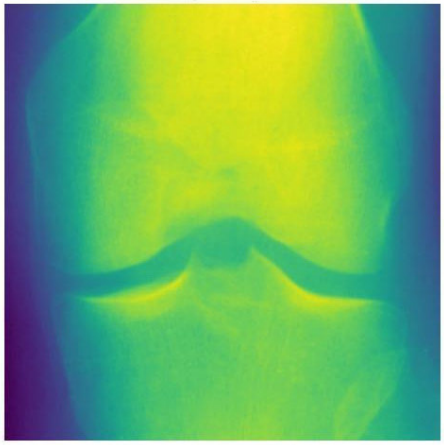

**FIGURE 2.** Preprocessed image of a Healthy Knee joint.

are frozen to retain essential feature representations from medical images, specifically focusing on patterns relevant to osteoarthritis (OA) severity. This feature extraction serves as the foundation for enhanced analysis of the subsequent quantum layer. The flow diagram of the quantum aspects of a quantum Convolutional Neural Network is depicted in Figure 3.

### C. QUANTUM LAYER INTEGRATION

A custom quantum convolutional layer was appended to the VGG16 model to leverage the unique capabilities of quantum computing. The principles of quantum feature representation guide the integration of a quantum convolutional layer into the VGG16 framework. Quantum circuits can encode classical image features into a high-dimensional Hilbert space through angle embedding and parameterized rotational gates (RX, RY, RZ), enabling complex nonlinear transformations. Entanglement via CNOT gates introduces correlations between qubits, allowing the model to capture complex feature dependencies across the image space. A custom quantum convolutional layer was appended to the VGG16 model to enhance feature representation beyond classical convolutional capacity. Unlike deepening a classical CNN, which increases parameter count and risks overfitting, quantum layers can achieve comparable or superior representational power with fewer parameters [2]. It is particularly beneficial for medical image classification, where subtle differences, such as early-stage OA indicators, may not be captured by classical depth alone. Earlier studies have demonstrated the effectiveness of Quantum CNNs in various biomedical

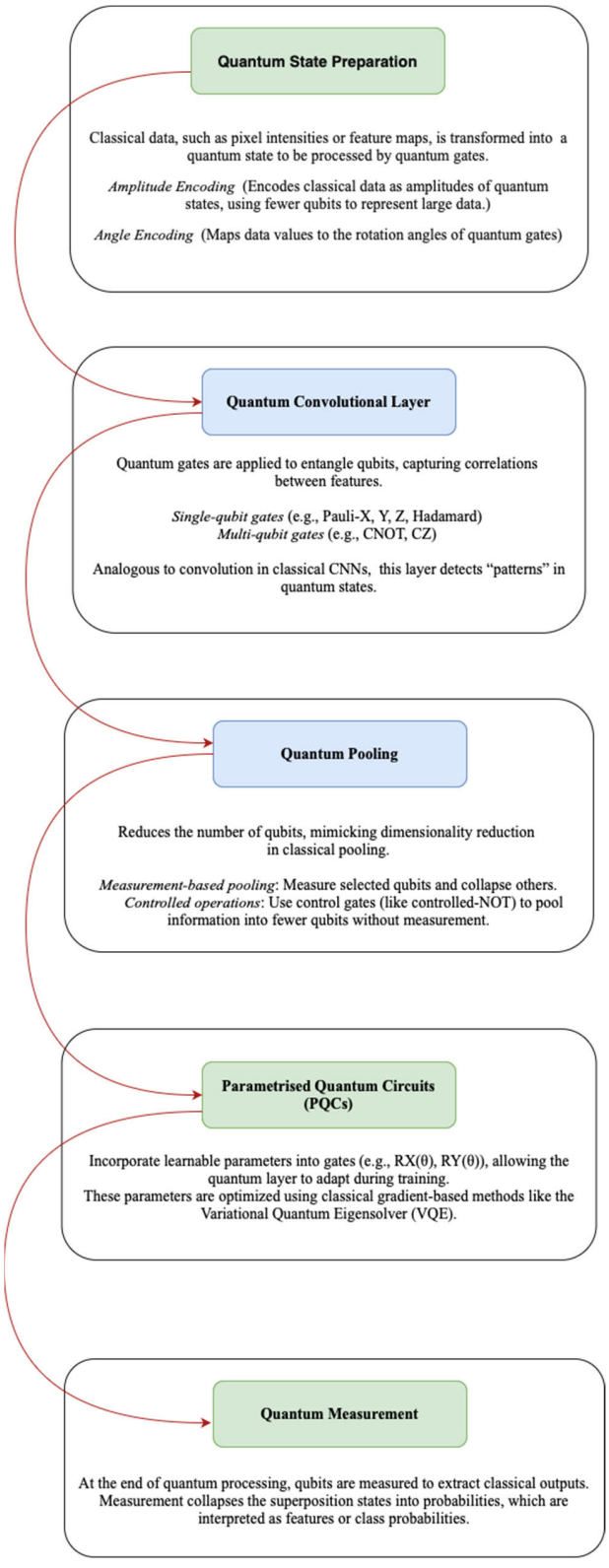


**FIGURE 3.** The flow diagram of the quantum aspects of a quantum convolutional neural network.

applications, including brain tumor classification [3] and ischemic cardiopathy detection [4], validating their theoretical suitability for OA diagnostics.

### D. ANGLE EMBEDDING

The input features x: [*x_0, x_1, x_2, x_3*] are encoded into the quantum circuit through rotations around the Y-axis R_Y for each qubit represented in Eq. (1):

$$R\_Y(\theta) = cos(\theta/2) - sin(\theta/2) \\ sin(\theta/2)cos(\theta/2) \quad (1)$$

For 4 qubits: $R\_Y(x\_0), R\_Y(x\_1), R\_Y(x\_2), R\_Y(x\_3)$

### E. STRONGLY ENTANGLING LAYERS

The strongly entangled layer consists of rotational gates and Controlled-NOT (CNOT) gates, applied in a specific pattern, to create entanglement.

Each qubit underwent parameterized rotations around the X-, Y-, and Z-axes:

$$R\_X(\phi), R\_Y(\theta), R\_Z(\lambda)$$

CNOT gates are applied between pairs of qubits:
CNOT *(q_i, q_{i+1}),* where $i = 0, 1, 2, \ldots$
For the four qubits, the entanglement sequence is:

$$CNOT(q\_0, q\_1) \\ CNOT(q\_1, q\_2) \\ CNOT(q\_2, q\_3) \\ CNOT(q\_3, q\_0)$$

Pauli-Z expectation values

The output of the quantum circuit was obtained by measuring the Pauli-Z expectation value for each qubit, as shown in Eq. (2):

$$< Z > \_i =< \psi | Z\_i | \psi > (2) \quad (2)$$

where Z_i is the Pauli-Z operator.

For 4 qubits are expressed in Eq. (3):

$$Output = [< Z > \_0, < Z > \_1, < Z > \_2, < Z > \_3] \quad (3)$$

### F. QUANTUM FEATURE EXTRACTION OUTPUT

The image is reduced to 4 key features are represented in Eq. (4):

$$x = [x\_0, x\_1, x\_2, x\_3] \quad (4)$$

The quantum circuit outputs the following values:
[-0.104, -0.051, 0.247, 0.256]

### G. USE OF THE SWISH ACTIVATION FUNCTION

The Swish activation function [25] is applied to the dense layers following the quantum convolutional layer. Swish was chosen for its ability to improve gradient flow and provide a smoother learning process, which is essential for handling complex, subtle features within medical images. This activation function enhances the capacity of the model to learn

**TABLE 3.** Hybrid OA_classification algorithm.

Input: $D_{s\rightarrow \text{OA-Dataset}}$

Output: $f(\text{label}) = \begin{cases} 0, & \text{if Healthy} \\ 1, & \text{if Affected} \end{cases}$

1. Given an image Img in dataset $D_s$, Img_i′=Resize (Img_i,(224,224)), where Img_i' is a resized image.
2. Img_i'=Img_i'/255,where Img_i'' is the normalized image of each pixel by pixel.
3. .Define function $f(\text{Label}) = \begin{cases} 0, & \text{if Healthy} \\ 1, & \text{if Affected} \end{cases}$
4. Label′={f(Label)| i = 1, 2, 3, ... N} ,where Label′ is a transformed label.
5. Extract features using Feature extraction Φ
   Φ(Img_i'') =G_AP (ReLU (Conv_ (Img_i''))),
   Where
   G_AP -Global_Average_Pooling
   ReLU - activation function
   Conv_ is Convolution.
6. Extracted_Feature_space, $f_s = \{\Phi (\text{Img\_i''}) \varphi \mid i = 1, 2, 3, \ldots N\}$
7. Quantum Feature Encoding
   define the angle embedding function
   $\theta_j = \pi \times ft_j$ , where $\theta_j$ is the quantum angle encoding for the feature $ft_j$.
   define quantum circuit Q(θ):
   Qubits= q, where q=4;
   For 4 qubits, the entanglement sequence is:
   CNOT (q_0, q_1)
   CNOT (q_1, q_2)
   CNOT (q_2, q_3)
   CNOT (q_3, q_0)
8. The quantum transformed features are Q(F)= Measurement (Unitary transformation(θ)).
9. Q(F) transformed using weight matrices, bias, and activation function.
10. Model training and optimization using Binary Cross entropy loss and Adam optimizer.
11. Model evaluation using performance metrics and final prediction has been done.

fine-grained differences, further boosting classification accuracy. The mathematical representation of the Swish function is mentioned in the following Eq. (5)

$$Swish(x) = x/(1 + e\text{^}(-\beta x)) \tag{5}$$

### H. CLASSIFICATION LAYER

After the feature extraction and quantum convolutional layers, the model includes a classification layer that categorizes knee images as ''Healthy'' or ''Affected'' based on OA severity. Probabilities are assigned to each class using a SoftMax function, which determines the likelihood that an image falls within each category.

## IV. EXPERIMENTAL SETUP

### A. DATASET DESCRIPTION

Knee osteoarthritis (OA) is a degenerative joint condition that results from the breakdown of cartilage within the knee. This cartilage usually provides a protective cushion between the bones, minimizing friction and impact during movement. As osteoarthritis progresses, the cartilage deteriorates, causing bones to rub against each other, leading to pain, stiffness, and reduced mobility. Over time, this condition can significantly affect the structure of joints and nearby tissues. Knee osteoarthritis is the most common type of arthritis associated with knee pain, with five different grade levels, as depicted in Figure 4, although other forms, such as rheumatoid arthritis and pseudogout, can also impact the knee.

This dataset [26] comprises knee X-ray images intended for knee joint detection and severity grading based on the Kellgren-Lawrence (KL) scale. To simplify the classification, the dataset was organized into two main categories:

*Healthy:*This category includes images of knees that display no signs of osteoarthritis with normal joint space and bone structure. These images serve as a reference for identifying healthy knee joints in the absence of osteoarthritis.

*Affected:*This category contains images of knees that show clear signs of advanced osteoarthritis, including joint space narrowing, bone density changes (sclerosis), and bone spur formation (osteophytes). These structural changes reflect significant cartilage breakdown and align with the symptoms of osteoarthritis, such as pain and limited mobility. The dataset is taken only for research purposes from and is structured for five grades as follows:

TRAINING SET CLASS DISTRIBUTION:
*Grade 0*: 2286 images
*Grade 1*: 1046 images
*Grade 2*: 1516 images
*Grade 3*: 757 images
*Grade 4*: 173 images
VALIDATION SET CLASS DISTRIBUTION:
*Grade 0*: 328 images
*Grade 1*: 153 images
*Grade 2*: 212 images
*Grade 3*: 106 images
*Grade 4*: 27 images
TEST SET CLASS DISTRIBUTION:
*Grade 0*: 639 images
*Grade*1: 296 images
*Grade 2*: 447 images
*Grade 3*: 223 images
*Grade* 4: 51 images
***TOTAL IMAGES IN THE DATASET: 8260***
*Train*: 5778 images
*Validation*: 826 images
*Test*: 1656 images

### B. TRAINING SETUP AND HYPERPARAMETERS

The proposed hybrid model was trained on a curated knee osteoarthritis (OA) radiograph dataset, which was divided into three grades of severity: grade 0 (normal), grade 3 (moderate), and grade 4 (severe). In the binary classification, grade 0 was assigned as class 0, and grades 3 and 4 were assigned

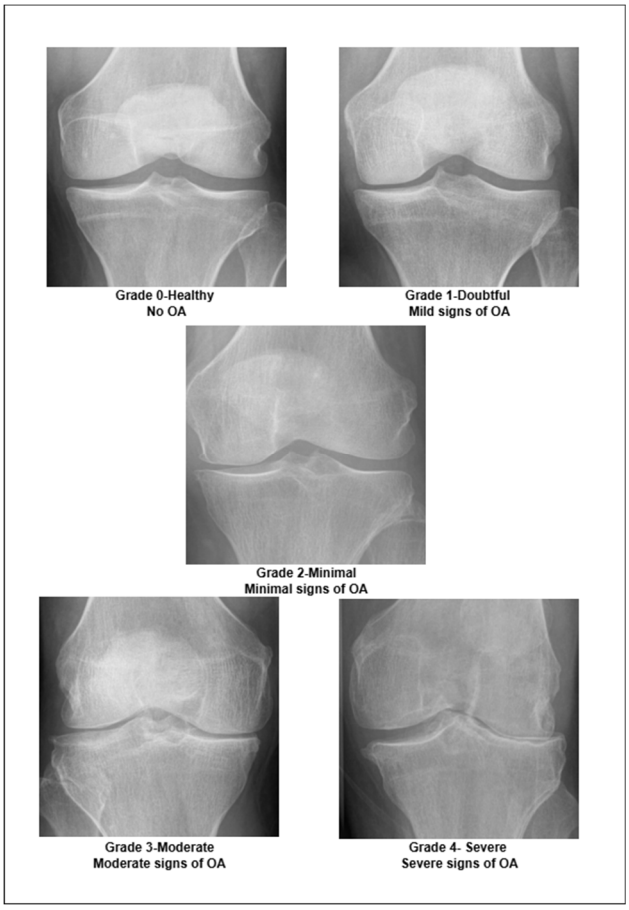


**FIGURE 4.** The five grades of knee OA, according to the given dataset.

as class 1. All images were resized to 224 × 224 pixels and normalized by dividing pixel intensity by 255.0. The dataset was divided into 3,216 training images, 461 for validation, and 913 for testing. The VGG16, pretrained on ImageNet, was used as a fixed feature extractor. The classification head was augmented with a custom quantum convolutional layer implemented using the PennyLane library. This quantum layer utilizes 4 qubits with angle embedding for input encoding and a circular entanglement structure (cyclic CNOT gates), which strikes a balance between computational feasibility and expressivity. These settings were chosen based on prior literature and validated through empirical experimentation. A small grid search has been made to choose stochastic gradient descent (SGD) with momentum 0.9.

An initial learning rate of $1 \times 10^{-3}$ has been chosen, and the learning rate was dynamically decreased using the ReduceLROnPlateau scheduler (factor: 0.2; patience: 5 epochs). Early stopping with patience (15 epochs) made use of restoring the best weights to prevent overfitting. Class imbalance was addressed using the calculated class weights. Sparse Categorical Cross-Entropy was employed as the loss function with classification accuracy as the primary evaluation metric. Training was carried out for a maximum of 50 epochs. A batch size of 64 was used throughout the experiments.

Parameter values such as batch size, learning rate schedule, and quantum circuit configuration were optimized through validation-based tuning and performance monitoring. Ablation studies on activation functions (ReLU vs. Swish) were also conducted to understand their influence. Experiments were performed on a Kaggle Kernel with dual NVIDIA T4 GPUs (16 GB VRAM each), and quantum simulations were performed using the default qubit backend in PennyLane. The total training time was approximately 10.43 minutes, with a peak change in memory usage of approximately 0.13 GB.

## V. RESULTS AND DISCUSSION

Upon testing our proposed model, we obtained positive results. All standard metrics were calculated to test the performance of the hybrid model. The highest testing accuracy for our proposed model was 97.26%, indicating a remarkable breakthrough in quantum convolution.

### A. EVALUATION METRICS

$$AccuracyHealthy = \frac{TPHealthy + TNHealthy}{TPHealthy + TNHealthy + FPHealthy + FNHealthy} \tag{6}$$

$$AccuracyAffected = \frac{TPAffected + TNAffected}{TPAffected + TNAffected + FPAffected + FNAffected} \tag{7}$$

$$PrecisionHealthy = \frac{TPHealthy}{TPHealthy + FPHealthy} \tag{8}$$

$$PrecisionAffected = \frac{TPAffected}{TPAffected + FPAffected} \tag{9}$$

$$RecallHealthy = \frac{TPHealthy}{TPHealthy + FNHealthy} \tag{10}$$

$$RecallAffected = \frac{TPAffected}{TPAffected + FNAffected} \tag{11}$$

$$F1\_scoreHealthy = 2.\left(\frac{precisionHealthy.recallHealthy}{precisionHealthy + recalHealthyl}\right) \tag{12}$$

$$F1\_scoreAffected = 2.\left(\frac{precisionAffected.recallAffected}{precisionAffected + recallAffected}\right) \tag{13}$$

Figure 5 shows the confusion matrix of the hybrid model, which explains the relationship between the actual and predicted outputs. True positive rates for Healthy and Affected classes were high, reflecting the balanced performance of the classification. Low misclassifications reflect good generalization.

Figures 6 and 7 show the comparison graphs between the training and validation of the hybrid model in terms of accuracy and loss, respectively.

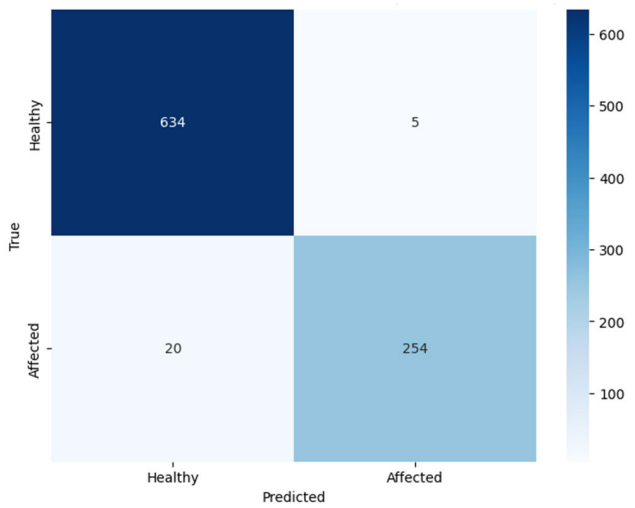


**FIGURE 5.** The confusion matrix for the predicted results between Label 0 and Label 1.


**FIGURE 6.** The training and validation accuracies over successive epochs.

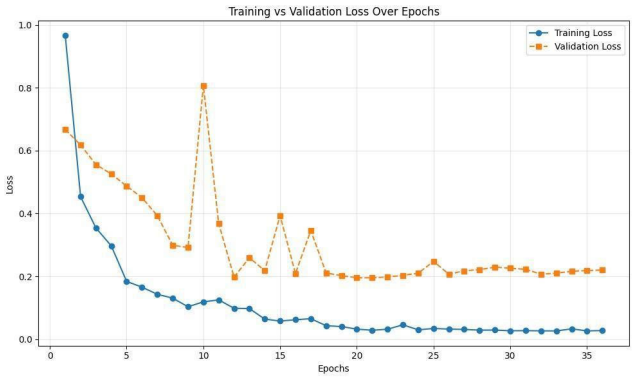


**FIGURE 7.** The training and validation Loss over successive epochs.

Figure 8 shows the Receiver Operating Characteristic (ROC) AUC of 0.9928, indicating an extremely high ability of the model to distinguish between healthy and affected knees.

Table 4, presents the remarkable results found for our proposed system, showing affirmative results for Accuracy, Precision, Recall and F1-Score.

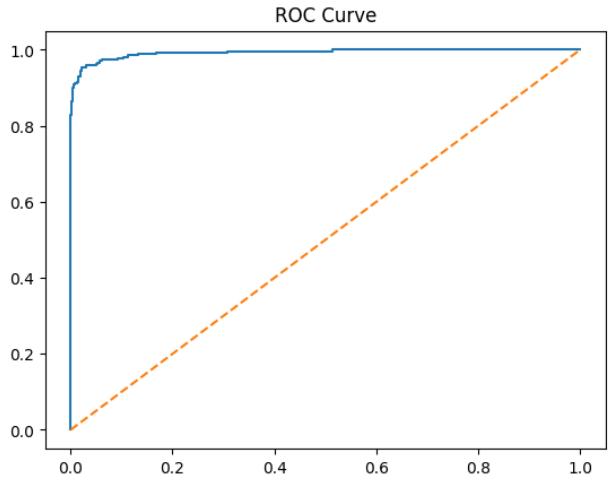


**FIGURE 8.** The AUC-ROC curve for the proposed model.

**TABLE 4.** Proposed model results.

| Class | Accuracy | Precision | Recall | F1 - Score |
|---|---|---|---|---|
| Healthy (Grade 0) | 0.97 | 0.97 | 0.98 | 0.97 |
| Affected (Grade 3 and 4) | 0.97 | 0.98 | 0.93 | 0.95 |
| Weighted Average | 0.97 | 0.97 | 0.96 | 0.97 |

### B. EPOCH-WISE MODEL IMPROVEMENT

To further substantiate our model's performance and its ability to learn disease-specific patterns, a comparison of predictions from early training (Epoch 3) versus later training (Epoch 4**3)** has been provided in Table 5. As shown in Figures 9 and 10, the top row represents the ground truth (T) and the bottom row shows the model predictions (P).

The visualization demonstrates the robustness of the model for accurately classifying knee X-ray images. During early training (epoch 3), the model misclassified all affected cases (T:1) as healthy (P = 0), indicating underfitting or insufficient learning of pathological features. Healthy samples (T:0) were correctly classified, but the model lacked the sensitivity to identify osteoarthritic changes. However, as shown in Figure 10, the model learned discriminative features better. It accurately classifies both healthy and affected knees with higher confidence. The true-positive rate has significantly improved, supported by a reduction in false negatives.

Error Analysis with Visual Evidence is shown in Figures 11a and 11b. Qualitative view of the remaining false positives and false negatives. These are borderline or subtle cases, suggesting that the remaining errors were due to intrinsic image ambiguity rather than model shortcomings.

### C. MODEL COMPARISON

The efficiency of the Hybrid model's classification ability was assessed in terms of training time and testing accuracy

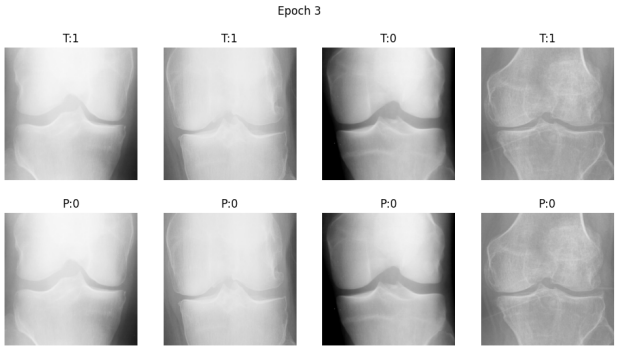


**FIGURE 9.** The epoch-wise model improvement- training at Epoch 3.

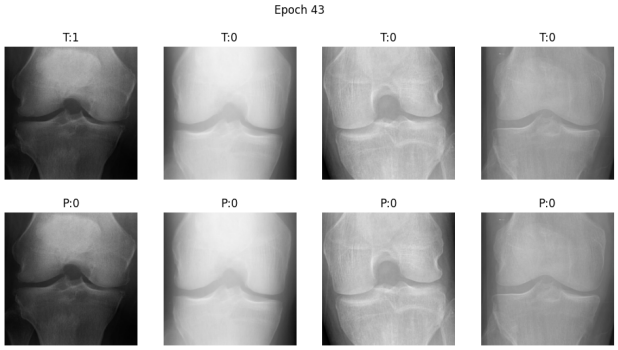


**FIGURE 10.** The epoch-wise model improvement- training at Epoch 43.

**TABLE 5.** Epoch-wise model improvement.

| Feature | Epoch3 (Figure 9) | Epoch 43 (Figure 10) |
|---|---|---|
| Affected Detection | Poor (all T:1 → P:0) | Improved (T:1 → P:1 matches) |
| False Negatives | High | Reduced |
| Feature Sensitivity | Low | High |
| Visual Agreement | Low | High |

with different combinations of activation functions utilized by different pre-trained models, such as InceptionNet, ResNet, and XceptionNet, using both ReLU and Swish activations combined with the QCNN. To ensure fairness, all models were trained on the same hardware (Kaggle Kernel with dual NVIDIA T4 GPUs, 16 GB VRAM), using identical training settings. These consistent conditions validate that observed performance gains are attributed to model architecture and not training variability.

### 1) INCEPTION-NET

Inception was a concept invented by Google that became part of the GoogLeNet family, revolutionizing deep learning in terms of modules that could process inputs at many scales simultaneously by combining convolutional layers. These

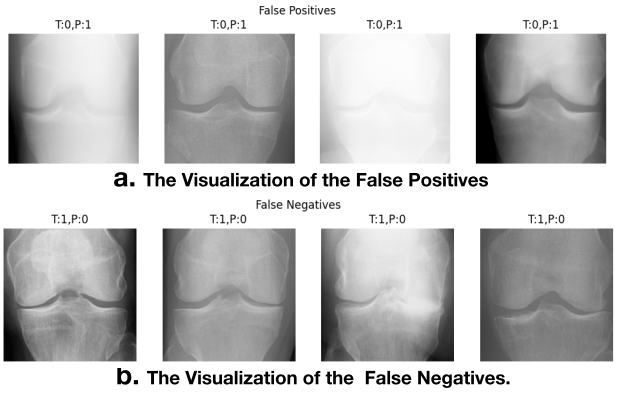


**FIGURE 11.** a. The Visualization of the False Positives b. The Visualization of the False Negatives.

layers have standard filter sizes of $1 \times 1$, $3 \times 3$, and $5 \times 5$ in parallel to solve the dilemma of which filter size is correct. It also relies on $1 \times 1$ convolutions to perform dimensionality reduction, in which the computational cost is further reduced without any loss of performance. Thus, InceptionNet delivers impressive accuracy using fewer parameters, making it a computationally efficient model for image recognition tasks [27].

### 2) RES-NET

Residual Networks (ResNet), developed by Microsoft, introduced the concept of ''residual learning.'' It was mainly developed to address the classical problem of vanishing gradients in neural networks. Instead of learning the unreferenced mappings, ResNet employs skip connections that can bypass one or more layers to learn the residual mappings. This also simplifies the optimization and enables the training of extremely deep networks including ResNet-50 and ResNet-101. The architecture has since become the gold standard for extracting features on computer vision tasks because of its ability to generalize well across datasets while maintaining computational efficiency [28].

### 3) XCEPTION-NET

XceptionNet was proposed as an extension of the InceptionNet. It substitutes traditional inception modules with depthwise separable convolutions to significantly improve performance and computational efficiency. This architecture separates the spatial and channel-wise feature extraction processes by first performing depthwise convolutions for spatial filtering, and then pointwise convolutions for combining channel-wise information. The architecture XceptionNet draws together both Inception and ResNet's best advantages and forms a simpler model but a more powerful version to carry out classification and image recognition with increased accuracy and few parameters [29].

Table 6 presents the comparative analysis of other model variations, showing the proposed model of VGG-16 and the QCNN model as a clear winner. The VGG16-QCNN

**TABLE 6.** Results comparison.

| Model | Activation | Test Accuracy (%) | Training Time (mins) |
|---|---|---|---|
| VGG16[30] | ReLU | 96.39 | 10.61 |
| VGG16+QCNN | Swish | **97.26** | 10.43 |
| XceptionNet[29] | ReLU | 87.84 | 7.03 |
| XceptionNet[29] | Swish | 86.09 | 6.69 |
| ResNet[28] | Swish | 89.70 | 8.40 |
| ResNet[28] | ReLU | 69.99 | 3.53 |
| InceptionNet[27] | ReLU | 86.86 | 3.75 |
| InceptionNet[27] | Swish | 86.64 | 4.35 |

**TABLE 7.** Ablation study.

| Model | Test Acc. | Precision | Recall | F1-Score | Train. Time (min) | Mem. (gb) |
|---|---|---|---|---|---|---|
| VGG16 + ReLU | 96.06 | 96 | 90 | 93 | 5.40 | 0.27 |
| VGG16+ Swish | 96.71 | 97 | 92 | 94 | 5.41 | 0.81 |
| Hybrid +ReLu | 96.39 | 96 | 94 | 94 | 10.61 | 0.18 |
| **Hybrid +Swish** | **97.26** | **98** | **93** | **95** | **10.43** | **0.13** |

with the Swish activation function not only outperforms other architectures in accuracy but also demonstrates superior computational efficiency, making it a practical and scalable solution for OA classification. Among the four models, this model yielded the highest test accuracy of 97.26%, indicating superior predictive performance.

It also trains efficiently with a time of 10.43 minutes, which is competitive with the other models. The memory usage is minimal at 0.13 GB, making it the most resource-efficient option. This combination would most likely exploit the strong feature extraction from VGG16, enriched representational power thanks to the activation of Swish, and the extra expressiveness of the quantum layer, making it the best choice for this classification problem.

#### 4) ABLATION STUDY

To assess the impact of activation functions and the integration of quantum convolutional layers, an ablation study was conducted across four model configurations: classical VGG16 with ReLU, VGG16 with Swish, hybrid VGG16-QCNN with ReLU, and hybrid VGG16-QCNN with Swish. Each model was trained on the same dataset, maintaining consistent training hyperparameters across all experiments.

Table 7 below summarizes the accuracy, precision, Recall, and F1-score for the affected class, as well as training time and memory usage. In the table, the hybrid name indicates VGG16 + QCNN. The results demonstrate that the hybrid QCNN with Swish achieved the highest test accuracy (97.26%) and other metrics for the affected class, outperforming the classical VGG16 with the same activation. The hybrid model achieves this with lower memory usage, which shows the enhanced representational efficiency due to quantum encoding and entanglement operations.

## VI. CONCLUSION

This work has explored only the beginning of the application of Quantum Convolution, thus far, seeing promising results. The most promising results were obtained with the combination of QCNN and VGG16 using the Swish activation function, which yielded an accuracy of 97.26%. This medical image classification of Osteoarthritis using Quantum Convolution can be a key application for the diagnosis of the disease, providing a breakthrough in AI-driven healthcare. Although the introduced hybrid VGG16-QCNN model shows strong performance in binary classification between healthy and OA-affected cases, such an assessment should be extended in the future to classify as multi class classification of osteoarthritis severity. In addition, reliance on simulated quantum circuits and focus on a single dataset raises the possibility that broader validation including multicenter data and eventual real-device implementation, could further confirm the model's clinical utility.

## REFERENCES


[1] C. P. Pal, P. Singh, S. Chaturvedi, K. K. Pruthi, and A. Vij, "Epidemiology of knee osteoarthritis in India and related factors," *Indian J. Orthopaedics*, vol. 50, no. 5, pp. 518–522, Oct. 2016, doi: 10.4103/0019-5413.189608.

[2] M. Schuld and N. Killoran, "Quantum machine learning in feature Hilbert spaces," *Phys. Rev. Lett.*, vol. 122, no. 4, Feb. 2019, Art. no. 040504, doi: 10.1103/physrevlett.122.040504.

[3] A. Senokosov, A. Sedykh, A. Sagingalieva, B. Kyriacou, and A. Melnikov, "Quantum machine learning for image classification," *Mach. Learn., Sci. Technol.*, vol. 5, no. 1, Mar. 2024, Art. no. 015040, doi: 10.1088/2632-2153/ad2aef.

[4] U. Ullah, A. G. O. Jurado, I. D. Gonzalez, and B. Garcia-Zapirain, "A fully connected quantum convolutional neural network for classifying ischemic cardiopathy," *IEEE Access*, vol. 10, pp. 134592–134605, 2022.

[5] X. Yang, W. Deng, and J. Yao, "Neural adaptive dynamic surface asymptotic tracking control of hydraulic manipulators with guaranteed transient performance," *IEEE Trans. Neural Netw. Learn. Syst.*, vol. 34, no. 10, pp. 7339–7349, Oct. 2023, doi: 10.1109/TNNLS.2022.3141463.

[6] R. Khanam, M. Hussain, R. Hill, and P. Allen, "A comprehensive review of convolutional neural networks for defect detection in industrial applications," *IEEE Access*, vol. 12, pp. 94250–94295, 2024, doi: 10.1109/ACCESS.2024.3425166.

[7] X. Yang, W. Deng, and J. Yao, "Neural network based output feedback control for DC motors with asymptotic stability," *Mech. Syst. Signal Process.*, vol. 164, Feb. 2022, Art. no. 108288, doi: 10.1016/j.ymssp.2021.108288.

[8] Z. Ping, Y. Xinying, and C. Zongji, "Neural network gain scheduling design for large envelope curve flight control law," *J. Beijing Univ. Aeronaut. Astronaut.*, vol. 31, no. 6, pp. 604–608, 2005.

[9] S. H. S. Almansour, R. Singh, S. M. H. Alyami, N. Sharma, M. S. A. Reshan, S. Gupta, M. F. M. Alyami, and A. Shaikh, "A convolution neural network design for knee osteoarthritis diagnosis using X-ray images," *Int. J. Online Biomed. Eng. (iJOE)*, vol. 19, no. 7, pp. 125–141, Jun. 2023, doi: 10.3991/ijoe.v19i07.40161.

[10] T. Tariq, Z. Suhail, and Z. Nawaz, "Knee osteoarthritis detection and classification using X-rays," *IEEE Access*, vol. 11, pp. 48292–48303, 2023, doi: 10.1109/ACCESS.2023.3276810.

[11] A. Brahim, R. Jennane, R. Riad, T. Janvier, L. Khedher, H. Toumi, and E. Lespessailles, "A decision support tool for early detection of knee OsteoArthritis using X-ray imaging and machine learning: Data from the OsteoArthritis initiative," *Computerized Med. Imag. Graph.*, vol. 73, pp. 11–18, Apr. 2019, doi: 10.1016/j.compmedimag.2019.01.007.

[12] J. D. D. Uwisengeyimana and T. I. T. Ibrik, "Diagnosing knee osteoarthritis using artificial neural networks and deep learning," *Biomed. Statist. Informat.*, vol. 2, no. 3, p. 95, 2017.
[13] R. K. Gebre, J. Hirvasniemi, R. A. van der Heijden, I. Lantto, S. Saarakkala, J. Leppilahti, and T. Jämsä, "Detecting hip osteoarthritis on clinical CT: A deep learning application based on 2-D summation images derived from CT," *Osteoporosis Int.*, vol. 33, no. 2, pp. 355–365, Feb. 2022, doi: 10.1007/s00198-021-06130-y.
[14] J.-B. Schiratti, R. Dubois, P. Herent, D. Cahané, J. Dachary, T. Clozel, G. Wainrib, F. Keime-Guibert, A. Lalande, M. Pueyo, R. Guillier, C. Gabarroca, and P. Moingeon, "A deep learning method for predicting knee osteoarthritis radiographic progression from MRI," *Arthritis Res. Therapy*, vol. 23, no. 1, p. 262, Dec. 2021, doi: 10.1186/s13075-021-02634-4.
[15] M. A. Khan, S. Kadry, P. Parwekar, R. Damaševičius, A. Mehmood, J. A. Khan, and S. R. Naqvi, "Human gait analysis for osteoarthritis prediction: A framework of deep learning and kernel extreme learning machine," *Complex Intell. Syst.*, vol. 9, no. 3, pp. 2665–2683, Jun. 2023, doi: 10.1007/s40747-020-00244-2.
[16] Y. Li, Y. Wang, X. Yang, and S.-K. Im, "Speech emotion recognition based on graph-LSTM neural network," *EURASIP J. Audio, Speech, Music Process.*, vol. 2023, no. 1, p. 40, Oct. 2023, doi: 10.1186/s13636-023-00303-9.
[17] K.-H. Chan, G. Pau, and S.-K. Im, "Chebyshev pooling: An alternative layer for the pooling of CNNs-based classifier," in *Proc. IEEE 4th Int. Conf. Comput. Commun. Eng. Technol. (CCET)*, Aug. 2021, pp. 106–110, doi: 10.1109/CCET52649.2021.9544405.
[18] K. Chan, S. Im, and W. Ke, "Variable-depth convolutional neural network for text classification," in *Proc. 27th ICONIP*, vol. 1333, Nov. 2020, pp. 685–692, doi: 10.1007/978-3-030-63823-8_78.
[19] S. S. Reka, H. L. Karthikeyan, A. J. Shakil, P. Venugopal, and M. Muniraj, "Exploring quantum machine learning for enhanced skin lesion classification: A comparative study of implementation methods," *IEEE Access*, vol. 12, pp. 104568–104584, 2024, doi: 10.1109/ACCESS.2024.3434681.
[20] P. Pitchal, S. Ponnusamy, and V. Soundararajan, "Heart disease prediction: Improved quantum convolutional neural network and enhanced features," *Expert Syst. Appl.*, vol. 249, Sep. 2024, Art. no. 123534, doi: 10.1016/j.eswa.2024.123534.
[21] A. Kodipalli, S. L. Fernandes, S. K. Dasar, and T. Ismail, "Computational framework of inverted fuzzy C-means and quantum convolutional neural network towards accurate detection of ovarian tumors," *Int. J. E-Health Med. Commun.*, vol. 14, no. 1, pp. 1–16, Apr. 2023, doi: 10.4018/ijehmc.321149.
[22] S. Chandra, S. Saxena, S. Kumar, M. K. Chaube, and N. K. Bodhey, "A novel framework for brain disease classification using quantum convolutional neural network," in *Proc. IEEE Int. Women Eng. (WIE) Conf. Electr. Comput. Eng. (WIECON-ECE)*, Dec. 2022, pp. 346–351, doi: 10.1109/WIECON-ECE57977.2022.10150851.
[23] B. Sriya, S. R. Warrier, and J. Dontabhaktuni, "Detection of brain cancer using quantum-classical CNN based method," in *Quantum Computing, Communication, and Simulation III*, vol. 12446, P. R. Hemmer and A. L. Migdall, Eds., SPIE, Mar. 2023, pp. 241–248, doi: 10.1117/12.2650132.
[24] A. R. Kesavapillai, S. M. Aslam, S. Umapathy, and F. Almutairi, "RA-XTNet: A novel CNN model to predict rheumatoid arthritis from hand radiographs and thermal images: A comparison with CNN transformer and quantum computing," *Diagnostics*, vol. 14, no. 17, p. 1911, Aug. 2024, doi: 10.3390/diagnostics14171911.
[25] P. Ramachandran, B. Zoph, and Q. V. Le, "Searching for activation functions," 2017, *arXiv.1710.05941*.
[26] P. Chen, "Knee osteoarthritis severity grading dataset," *Mendeley Data*, vol. V1, Sep. 2018, doi: 10.17632/56rmx5bjcr.
[27] C. Szegedy, W. Liu, Y. Jia, P. Sermanet, S. Reed, D. Anguelov, D. Erhan, V. Vanhoucke, and A. Rabinovich, "Going deeper with convolutions," in *Proc. IEEE Conf. Comput. Vis. Pattern Recognit. (CVPR)*, Jun. 2015, pp. 1–9, doi: 10.1109/CVPR.2015.7298594.
[28] K. He, X. Zhang, S. Ren, and J. Sun, "Deep residual learning for image recognition," in *Proc. IEEE Conf. Comput. Vis. Pattern Recognit. (CVPR)*, Jun. 2016, pp. 770–778, doi: 10.1109/CVPR.2016.90.
[29] F. Chollet, "Xception: Deep learning with depthwise separable convolutions," in *Proc. IEEE Conf. Comput. Vis. Pattern Recognit. (CVPR)*, Jul. 2017, pp. 1800–1807, doi: 10.1109/CVPR.2017.195.
[30] K. Simonyan and A. Zisserman, "Very deep convolutional networks for large-scale image recognition," 2014, *arXiv.1409.1556*.

**DEVANSH TIKARIHA** is currently pursuing the bachelor's degree with the School of Computer Science and Engineering, Vellore Institute of Technology(VIT), Chennai, specializing in artificial intelligence and machine learning. His major research interests include deep neural networks and generative AI.

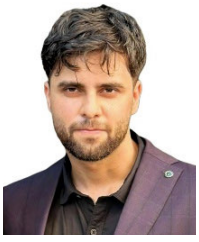

**ABDUL MOOMIN** is currently pursuing the bachelor's degree with the School of Computer Science and Engineering, Vellore Institute of Technology(VIT), Chennai, specializing in artificial intelligence and machine learning. His major research interests include deep neural networks and generative AI.

**D. JEYAMANI** received the M.E. degree in computer science and engineering from Annamalai University, in 2012. He is currently pursuing the Ph.D. degree with the School of Computer Science and Engineering, Vellore Institute of Technology (VIT), Chennai. He is a full-time Research Scholar with the School of Computer Science and Engineering, VIT. His research interests include biomedical data analytics and medical image processing.

**P. RUKMANI** received a PhD in the School of Computer Science and Engineering from the Vellore Institute of Technology (VIT), in 2017. She has completed her M. Tech in Information Technology from Anna University. She is currently working as a Professor at the School of Computer Science and Engineering, VIT, Chennai Campus. Her research areas include Scheduling Algorithms, QoS for Wireless Networks, the Internet of Things (IoT), Machine Learning, and Cybersecurity.